This is the accepted manuscript made available via CHORUS. The article has been published as:

Virial series expansion and Monte Carlo studies of equation of state for hard spheres in narrow cylindrical pores

K. K. Mon

Phys. Rev. E **97**, 052114 — Published 14 May 2018

DOI: 10.1103/PhysRevE.97.052114

Virial series expansion and Monte Carlo studies of equation of state for hard spheres in narrow cylindrical pores

K. K. Mon[1, a)]

Department of Physics and Astronomy, University of Georgia, Athens, Georgia 30602, USA

(Dated:)

In this paper, virial series expansion and constant pressure Monte Carlo method are used to study the longitudinal pressure equation of state for hard spheres in narrow cylindrical pores. We invoke dimensional reduction and map the model into an effective one dimensional fluid model with interacting internal degrees of freedom. The one dimensional model is extensive. Euler relation holds and longitudinal pressure can be probed with standard virial series expansion method. Virial coefficients B_2 and B_3 were obtained analytically and numerical quadrature was used for B_4. A range of narrow pore widths ($2R_p$), $R_p < (\sqrt{3}+2)/4 = 0.9330...$ (in units of the hard sphere diameter) was used, corresponding to fluids in the important single-file formations. We have also computed the virial pressure series coefficients B_2', B_3' and B_4' to compare a truncated virial pressure series equation of state with new accurate constant pressure Monte Carlo data. We find very good agreements for a wide range of pressures for narrow pores. These new results contribute toward increasing the rather limited understanding of virial coefficients and equation of state of hard sphere fluids in narrow cylindrical pores.

PACS numbers: 05.20.Jj, 05.70.Ce

[a)]Electronic mail: kkmon@hal.physast.uga.edu

I. INTRODUCTION

Thermodynamics of fluids in narrow pores and the crossovers from the one dimensional limit have been a subject of long standing interests[1–13] but much more remains basically unsolved. In this paper, we use the virial expansion method to study hard sphere fluid in very narrow cylindrical pores. Virial expansion has been used extensively to study interacting fluids.[14–19] For the bulk fluids, many virial coefficients[14–19] can be evaluated. This is especially true for hard sphere fluids. Analytical results have been obtained in low and high dimensions for hard spheres.[14–24] There are also much interests in applications of virial series expansions to inhomogeneous fluids with surfaces and walls.[25]

The second virial coefficient for hard disks in narrow hard channels have been computed analytically.[9,11,12] For homogeneous fluids in very narrow cylindrical pores, much less is known. There are some numerical results for the second virial coefficients for hard spheres in cylindrical pores [9]. The third and fourth virial coefficients of hard spheres in cylindrical pores are basically unexplored. In this paper, we have evaluated them. Virial coefficients B_2 and B_3 were obtained analytically and numerical quadrature was used for B_4. A range of narrow pore widths ($2R_p$), $R_p < (\sqrt{3}+2)/4 = 0.9330...$ (in units of the hard sphere diameter) was used, corresponding to fluids in the important single-file formations. They correspond to three dimensional single file fluids with only nearest-neighbor interactions and is of some interests.[26]

We have also computed the virial pressure series coefficients B_2', B_3' and B_4' to compare a truncated virial pressure series equation of state with new accurate constant pressure Monte Carlo data. We find very good agreements for a wide range of pressures for narrow pores. These new results contribute toward increasing the rather limited understanding of virial coefficients and equation of state of hard sphere fluids in narrow cylindrical pores.

In section II, Euler relation, dimensional reduction and the method of virial expansion for hard spheres in cylindrical pores will be discussed. Computational techniques are considered in section III. The virial expansion equation of states are compared to new accurate Monte Carlo data in section IV and the paper ends with some remarks in section V.

II. DIMENSIONAL REDUCTION, EULER RELATION AND VIRIAL SERIES EXPANSION

In this section, we will review the dimensional reduction analysis to show that fluids in narrow cylindrical pores can be reduced to an effectively one dimensional fluid model. It is extensive in the longitudinal length L and the longitudinal pressure can be studied with standard virial series expansion method. We will take the dimensional reduction approach, related to that used by Post and Kofke[4] . See also, Glandt[2].

The hard spheres are in narrow cylindrical pores with the length of the pore taken to the thermodynamic limit ($N, L \to \infty$). The linear number density is fixed at $l^{-1} = N/L$. One starts by rewriting the partition function,

$$Q_N(V,T) = \frac{1}{N!\Lambda^{3N}} \int_0^L dz_1 ... \int_0^L dz_N$$

$$\times \left\{ \int_0^{\hat{R}} r_1 dr_1 \int_0^{2\pi} d\theta_1 ... \int_0^{\hat{R}} r_N dr_N \int_0^{2\pi} d\theta_N \quad exp(-\beta U(r_1, \theta_1, z_1 ..., r_N, \theta_N, z_N)) \right\}.$$

$$= \frac{1}{N!\Lambda^{3N}} \int_0^L dz_1 ... \int_0^L dz_N \times W_{eff}(\hat{R}, z_1, ..., z_N) \tag{1}$$

$$W_{eff}(\hat{R}, z_1, ..., z_N) = \left\{ \int_0^{\hat{R}} r_1 dr_1 \int_0^{2\pi} d\theta_1 ... \int_0^{\hat{R}} r_N dr_N \int_0^{2\pi} d\theta_N \quad exp(-\beta U(r_1, \theta_1, z_1 ..., r_N, \theta_N, z_N)) \right\}. \tag{2}$$

$\hat{R} = R_p - \frac{1}{2}$ and Λ is the thermal deBroglie wavelength. Lengths are in units of the hard sphere diameter, $\sigma_{hs} = 1$ and U is the sum of nearest-neighbor hard sphere potentials. W_{eff} in general is complicated (see Post and Kofke[4]), but we do not need to evaluate it for our analysis.

For fixed $\hat{R}$, and constant linear number density $l^{-1} = N/L$, there is only one spatial extensive parameter L. The transverse lengths are fixed and do not scale with N. Thus, this model is one dimensional, extensive in the longitudinal direction and the pressure is anisotropic.

$$Q_N(V = \pi\hat{R}^2 L, T) = Q_N(L, \hat{R}, T) = Q_N(L, T) \tag{3}$$

It then follows from Euler's theorem that the longitudinal pressure P_L is related to the grand partition function Ξ as,

$$\beta P_L = \frac{1}{V} ln\Xi = \frac{1}{\pi\hat{R}^2 L} ln\Xi, \tag{4}$$

$\beta = 1/k_B T$. For the partition function, one apply the Mayer cluster integral expansion method (see reference 14) to obtain,

$$\Xi(\mu, T, L) = exp\left(\pi\hat{R}^2 L \sum_{k=0}^{\infty} \xi^k b_k(T)\right). \tag{5}$$

$b_k(T)$ are the cluster integrals,

$$b_k(T) = lim_{L\to\infty} \quad \frac{1}{k!\pi\hat{R}^2 L} \int_V d^3\mathbf{r_1}...d^3\mathbf{r_k} U_k(\mathbf{r_1}, ..., \mathbf{r_N}). \tag{6}$$

$U_k(\mathbf{r_1}, ..., \mathbf{r_N})$ are the Ursell functions defined as the sum of all connected numbered Mayer graphs of k points[14]. We have introduced the fugacity ξ in terms of absolute activity $\lambda = exp(\beta\mu)$, chemical potential μ and thermal deBroglie wavelength Λ ,

$$\xi = \frac{\lambda}{\Lambda^3} \tag{7}$$

This reduces to,

$$\beta P_L = \sum_{k=0}^{\infty} \xi^k b_k(T) \tag{8}$$

.

In the grand ensemble, the average number of particles in the system is :

$$N = k_B T \frac{\partial ln\Xi}{\partial\mu}\bigg|_{V,T} = \lambda \frac{\partial ln\Xi}{\partial\lambda}\bigg|_{V,T} = \pi\hat{R}^2 L \sum_{k=0}^{\infty} k\xi^k b_k(T) \tag{9}$$

.

The number density ρ is,

$$\rho = \frac{N}{\pi \hat{R}^2 L} = \sum_{k=0}^{\infty} k \xi^k b_k(T) \tag{10}$$

.

A virial series for the longitudinal pressure βP_L in terms of density ρ can be introduced,

$$\beta P_L = \rho(1 + B_2^{(\rho)}\rho + B_3^{(\rho)}\rho^2 + B_4^{(\rho)}\rho^3 + ...). \tag{11}$$

To obtain equation for the virial coefficients $B_n^{(\rho)}$, start by eliminating ρ with equation 10. Then, by equating it to equation 8 for βP_L will lead to,

$$B_{k+1}^{(\rho)} = -\frac{k}{k+1}\beta_k. \tag{12}$$

$B_{k+1}^{(\rho)}$ are the virial coefficients and β_k are the irreducible cluster integrals. For a good reference, see McCoy[14].

This shows that we can apply the standard virial series expansion method to study the longitudinal pressure P_L of fluids in cylindrical pores. Since Euler relation does not hold for the transverse length scale which is not extensive, the way to study the transverse pressure is different. It has to be computed by taking appropriate derivative of the free energy and will be considered elsewhere.

Since $\hat{R}$ is a constant, ρ is related to l^{-1} as,

$$\rho = \frac{N}{\pi \hat{R}^2 L} = \frac{1}{\pi \hat{R}^2}\frac{N}{L} = \frac{1}{\pi \hat{R}^2} l^{-1} \tag{13}$$

.

Now eq (11) can be rewritten as a virial expansion for an one dimensional system with linear density l^{-1},

$$\beta p = l^{-1}(1 + B_2 l^{-1} + B_3 l^{-2} + B_4 l^{-3} + ...). \tag{14}$$

$p = P_L \pi \hat{R}^2$ is the linear pressure for the equivalent one dimensional system with one dimensional density virial expansion coefficients B_n defined by,

$$B_n = \frac{B_n^{(\rho)}}{(\pi \hat{R}^2)^{n-1}}. \tag{15}$$

III. EVALUATION OF VIRIAL COEFFICIENTS: B_2, B_3, B_4

There are some numerical estimates[9] for the B_2 but no virial coefficients of hard spheres in cylindrical pores are known to have been calculated analytically. We have evaluated B_2 and B_3 analytically. Parts of the multi-integrals can be done in closed form and the remaining by expanding in a power series and integrating term by term analytically.
The second virial coefficient in the ρ series expansion is,

$$B_2^{(\rho)} = \frac{-1}{2V}\int dv_1 \int dv_2 \quad f_{12}$$

$$= \frac{-1}{2V}\int_0^{\hat{R}} r_1 dr_1 \int_0^{2\pi} d\theta_1 \int_0^{\hat{R}} r_2 dr_2 \int_0^{2\pi} d\theta_2 \int_0^{L} dz_1 \int_0^{L} dz_2 \quad f_{12}.$$

$$= \frac{-2\pi}{2(\pi\hat{R}^2)}\int_0^{2\pi} d\theta_{12} \int_0^{\hat{R}} r_1 dr_1 \int_0^{\hat{R}} r_2 dr_2 \int_{-1}^{1} dz_{12} \quad f_{12} \tag{16}$$

with,

$$f_{12} \equiv f_{12}(r_{12}) = e^{-\beta V_{hs}(r_{12})} - 1. \tag{17}$$

$\hat{R} = R_p - \frac{1}{2}, \theta_{12} = |\theta_1 - \theta_2|, r_{12} = |\vec{r}_1 - \vec{r}_2| = \sqrt{z_{12}^2 + r_1^2 + r_2^2 - 2r_1 r_2 cos(\theta_{12})}$ and $V_{hs}(r_{12})$ is the hard sphere potential.
Then, the one dimensional virial expansion coefficients for B_2 is,

$$B_2 = \frac{B_2^{(\rho)}}{(\pi\hat{R}^2)} = \frac{-2\pi}{2(\pi\hat{R}^2)^2}\int_0^{2\pi} d\theta_{12} \int_0^{\hat{R}} r_1 dr_1 \int_0^{\hat{R}} r_2 dr_2 \int_{-1}^{1} dz_{12} \quad f_{12} \tag{18}$$

This corresponds to the Ree-Hoover diagram[18] of figure 1a.

The integration over z_{12} is elementary,

$$\int_{-1}^{1} dz_{12} f_{12} = -2\sqrt{1 - \epsilon_{12}(r_1, r_2, \theta_{12})}, \tag{19}$$

with

$$\epsilon_{ij}(r_i, r_j, \theta_{ij}) = (r_i^2 + r_j^2 - 2r_i r_j cos(\theta_{ij})). \tag{20}$$

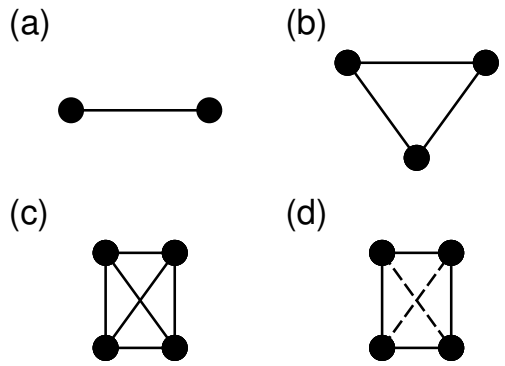

FIG. 1. Ree-Hoover diagrams for virial coefficients. (a): B_2, (b): B_3, (c): $\tilde{S}_1$ for B_4, (d): $\tilde{S}_2$ for B_4. The solid lines denote the Mayer f_{ij} function and dashed lines denote $\tilde{f}_{ij} = 1 + f_{ij}$.

One can expand the $\sqrt{1-\epsilon_{12}}$ in a power series of ϵ_{12},

$$\sqrt{1-\epsilon_{12}} = \sum_{n=0}^{\infty} \frac{(2n)!}{(1-2n)(n!)^2(4^n)}(\epsilon_{12})^n. \tag{21}$$

Each term can be integrated exactly to yield a power series in powers of $\hat{R}$ with,

$$B_2(\hat{R}) = 1 - \frac{1}{2}\hat{R}^2 - \frac{5}{24}\hat{R}^4 - \frac{7}{32}\hat{R}^6 - \frac{21}{64}\hat{R}^8 - \frac{77}{128}\hat{R}^{10}$$

$$-\frac{1287}{1024}\hat{R}^{12} - \frac{23595}{8192}\hat{R}^{14} - \frac{347633}{49152}\hat{R}^{16} - \frac{600457}{32768}\hat{R}^{18} - \frac{6495853}{131072}\hat{R}^{20}$$

$$-\frac{218360597}{1572860}\hat{R}^{22} - \frac{419924225}{1048576}\hat{R}^{24} - \frac{2483551845}{2097152}\hat{R}^{26} - \frac{120038339175}{33554432}\hat{R}^{28}$$

$$-\frac{5910122934675}{536870912}\hat{R}^{30} - \frac{36967239532575}{1073741824}\hat{R}^{32} - \frac{234558215747625}{2147483648}\hat{R}^{34} \quad . \quad . \quad . \tag{22}$$

More terms can be easily calculated with the help of symbolic computations. Convergence is rapid and we have checked it with numerical integrations. For example, with $\hat{R} = 0.4$, equation 22 yields 0.91345843 versus 0.91345844 from numerical quadrature. The uncertainty is in the last digit.

The third virial coefficient also has only one Ree-Hoover diagram (figure 1b),

$$B_3^{(\rho)} = \frac{-1}{3V} \int dv_1 \int dv_2 \int dv_3 \quad f_{12} f_{13} f_{23} \tag{23}$$

and

$$B_3 = \frac{-2\pi}{3(\pi \hat{R}^2)^3} \int_0^{2\pi} d\theta_{12} \int_0^{2\pi} d\theta_{13} \int_0^{\hat{R}} r_1 dr_1 \int_0^{\hat{R}} r_2 dr_2 \int_0^{\hat{R}} r_3 dr_3$$
$$\times \int_{-1}^{1} dz_{12} f_{12} \int_{-1}^{1} dz_{13} f_{13} f_{23}. \tag{24}$$

$\theta_{ij} = |\theta_i - \theta_j|, r_{ij} = |\vec{r_i} - \vec{r_j}| = \sqrt{z_{ij}^2 + r_i^2 + r_j^2 - 2 r_i r_j cos(\theta_{ij})}$.

The integrations over z_{12}, z_{13} can be done analytically and denoted as -**A**,

$$-\mathbf{A} \equiv \int_{-1}^{1} dz_{12} f_{12} \int_{-1}^{1} dz_{13} f_{13} f_{23}. \tag{25}$$

$$\mathbf{A} = 2(\sigma_c \sigma_b + \sigma_a \sigma_c + \sigma_a \sigma_b) - (\sigma_a^2 + \sigma_b^2 + \sigma_c^2). \tag{26}$$

$$\sigma_a = \sigma_{12}, \sigma_b = \sigma_{13}, \sigma_c = \sigma_{23}. \tag{27}$$

$$\sigma_{ij} = \sqrt{1 - \epsilon_{ij}}. \tag{28}$$

and

$$B_3 = \frac{2\pi}{3(\pi \hat{R}^2)^3} \int_0^{2\pi} d\theta_{12} \int_0^{2\pi} d\theta_{13} \int_0^{\hat{R}} r_1 dr_1 \int_0^{\hat{R}} r_2 dr_2 \int_0^{\hat{R}} r_3 dr_3$$

$$\times [2(\sigma_c \sigma_b + \sigma_a \sigma_c + \sigma_a \sigma_b) - (\sigma_a^2 + \sigma_b^2 + \sigma_c^2)]. \tag{29}$$

By symmetry, there are only two types of integrals to do,

$$\mathbf{B} = \int_0^{2\pi} d\theta_{12} \int_0^{2\pi} d\theta_{13} \int_0^{\hat{R}} r_1 dr_1 \int_0^{\hat{R}} r_2 dr_2 \int_0^{\hat{R}} r_3 dr_3 \sigma_\alpha \sigma_\beta, \quad \alpha \neq \beta. \tag{30}$$

$$\mathbf{C} = \int_0^{2\pi} d\theta_{12} \int_0^{2\pi} d\theta_{13} \int_0^{\hat{R}} r_1 dr_1 \int_0^{\hat{R}} r_2 dr_2 \int_0^{\hat{R}} r_3 dr_3 (\sigma_\alpha)^2. \tag{31}$$

C can be evaluated in closed form as,

$$\mathbf{C} = \frac{\pi^2 \hat{R}^6}{2}(1 - \hat{R}^2). \tag{32}$$

The **B** term appears to be different and has to be calculated as for B_2 by expanding the $\sqrt{.....}$ and integrate term by term to yield a power series in $\hat{R}$. The final result for B_3 is,

$$B_3(\hat{R}) = 1 - \hat{R}^2 - \frac{7}{24}\hat{R}^4 - \frac{19}{48}\hat{R}^6 - \frac{65}{96}\hat{R}^8 - \frac{1291}{960}\hat{R}^{10}$$

$$-\frac{6073}{2048}\hat{R}^{12} - \frac{1822885}{258048}\hat{R}^{14} - \frac{3072455}{172032}\hat{R}^{16} - \frac{13960009}{294912}\hat{R}^{18} - \frac{2306857403}{17694720}\hat{R}^{20}$$

$$-\frac{3206519887}{8650752}\hat{R}^{22} - \frac{18728895875}{17301504}\hat{R}^{24} - \frac{88185547953}{27262976}\hat{R}^{26} - \frac{361234293689153}{36641439744}\hat{R}^{28}$$

$$-\frac{287223536237301}{9395240960}\hat{R}^{30} - \frac{155026303764017}{1610612736}\hat{R}^{32} - \frac{33641701357295089}{109521666048}\hat{R}^{34}$$

$$-\frac{434647739535045095}{438086664192}\hat{R}^{36} - \frac{1057439817596234513}{326417514496}\hat{R}^{38} \quad . \quad . \quad . \tag{33}$$

Again, more terms can be easily calculated with the help of symbolic computations. Convergence is also rapid and we have checked it with numerical integrations. For example, with

$\hat{R} = 0.4$, equation 33 yields 0.830244942 versus 0.830248 from numerical quadrature. The uncertainty is in the last digit for the numerical integration. The terms decreases rapidly and the last term shown in equation 33 contributes a small value of 0.000000002 .

The fourth virial coefficient has two Ree-Hoover diagrams. The first diagram $\tilde{S}_1$ (figure 1c) contributes,

$$B_{4a} = \frac{2\pi}{4(\pi\hat{R}^2)^4} \int_0^{2\pi} d\theta_{12} \int_0^{2\pi} d\theta_{13} \int_0^{2\pi} d\theta_{14}$$

$$\times \int_0^{\hat{R}} r_1 dr_1 \int_0^{\hat{R}} r_2 dr_2 \int_0^{\hat{R}} r_3 dr_3 \int_0^{\hat{R}} r_4 dr_4$$

$$\times \int_{-1}^{1} f_{12} dz_{12} \int_{-1}^{1} f_{13} f_{23} dz_{13} \int_{-1}^{1} f_{14} f_{24} f_{34} dz_{14}. \tag{34}$$

The second Ree-Hoover diagram $\tilde{S}_2$ (figure 1d) is denoted as B_{4b}. In these diagrams, the solid lines denote the Mayer f_{ij} functions and dashed lines denote $\tilde{f}_{ij} = 1 + f_{ij}$. Both diagrams contribute to $B_4 = B_{4a} + B_{4b}$.

$$B_{4b} = -\frac{3}{8}[\frac{2\pi}{(\pi\hat{R}^2)^4}] \int_0^{2\pi} d\theta_{12} \int_0^{2\pi} d\theta_{13} \int_0^{2\pi} d\theta_{14}$$

$$\times \int_0^{\hat{R}} r_1 dr_1 \int_0^{\hat{R}} r_2 dr_2 \int_0^{\hat{R}} r_3 dr_3 \int_0^{\hat{R}} r_4 dr_4$$

$$\times \int_{-1}^{1} f_{12} dz_{12} \int_{-1}^{1} \tilde{f}_{13} f_{23} dz_{13} \int_{-1}^{1} f_{14} \tilde{f}_{24} f_{34} dz_{14}. \tag{35}$$

For now, we are not able to reduce the B_4 calculations to be suitable for symbolic computations. To provide estimates which will be useful for future analytical calculations, we have used numerical Gaussian integrations [27] for 9 different values of $\hat{R}$. See table 1. The number of Gaussian integration points used for each integral (≤ 1000) was varied and extrapolated to the large number limits. We have checked our numerical method by using the same routines to obtain estimates for B_2 and B_3 . As noted above they are in good agreements with our analytic results.

We have also computed the virial pressure series coefficients B_2', B_3' and B_4' to compare a

TABLE I. Second, Third and Fourth Virial Coefficients for hard spheres in cylindrical pores with widths $2R_p$. $R_p = \frac{1}{2}$ is the exactly soluble hard rod model[28] and all virial coefficients are 1. For $R_p > \frac{1}{2}$, B_2, B_3 are analytic predictions of equations 22 and 23 , respectively. B_4 are extrapolated values from numerical integrations with $B_4 = B_{4a} + B_{4b}$. For B_4, the last two digits are uncertain. The magnitude of the uncertainties are in parentheses. The pressure virial series B_3', B_4' from equations 40, 39, respectively are also shown.

R_p	B_2	B_3	B_3'	B_4	B_4'
$\frac{1}{2}$	1	1	0	1	0
0.52	0.999 799 966..	0.999 599 95..	-0.000 000 02..	0.999 3130 (10)	-0.000 000 (01)
0.55	0.998 748 694..	0.997 498 17..	-0.000 000 78..	0.996 2235 (06)	-0.000 000 (01)
0.60	0.994 978 944..	0.989 970 43..	-0.000 012 67..	0.984 9752 (05)	-0.000 000 (01)
0.65	0.988 641 951..	0.977 347 65..	-0.000 065 25..	0.966 1182 (15)	-0.000 000 (02)
0.70	0.979 651 759..	0.959 506 11..	-0.000 211 45..	0.939 5689 (15)	-0.000 000 (02)
0.75	0.967 877 124..	0.936 252 21..	-0.000 533 91..	0.905 1441 (10)	-0.000 000 (01)
0.80	0.953 127 105..	0.907 294 55..	-0.001 156 72..	0.862 5625 (30)	-0.000 000 (03)
0.85	0.935 125 123..	0.872 191 66..	-0.002 267 33..	0.811 3642 (30)	-0.000 004 (03)
0.90	0.913 458 430..	0.830 244 94..	-0.004 161 36..	0.750 7733 (10)	-0.000 018 (01)

truncated virial pressure series equation of state with new accurate constant pressure Monte Carlo data. The virial pressure series is defined as,

$$\beta pl = 1 + B_2'(\hat{R})(\beta p) + B_3'(\hat{R})(\beta p)^2 + B_4'(\hat{R})(\beta p)^3 + ..., \tag{36}$$

The virial pressure series coefficients B_n' has been tabulated[29] in terms of the virial density series coefficients B_n,

$$B_2' = B_2, \tag{37}$$

$$B_3' = B_3 - B_2^2, \tag{38}$$

$$B_4' = B_4 - 3B_2B_3 + 2B_2^3. \tag{39}$$

See reference 29. Note that $B_2'(\hat{R})$ is given by $B_2(\hat{R})$.

Using our analytic results for B_2, B_3 equations 22 and 23, analytic predictions for B_3' is,

$$B_3'(\hat{R}) = -\frac{1}{8}\hat{R}^4 - \frac{1}{6}\hat{R}^6 - \frac{163}{576}\hat{R}^8 - \frac{359}{640}\hat{R}^{10} - \frac{2535}{2048}\hat{R}^{12} - \frac{47653}{16128}\hat{R}^{14}$$

$$-\frac{429469}{57344}\hat{R}^{16} - \frac{1467523}{73728}\hat{R}^{18} - \frac{486331999}{8847360}\hat{R}^{20} - \frac{533012339566313}{3401605447680}\hat{R}^{22} - \frac{2080614548599833}{4535473930240}\hat{R}^{24}$$

$$-\frac{5891402846511563}{4288084443136}\hat{R}^{26} - \frac{60459844952626018709}{14407963728936960}\hat{R}^{28} - \frac{602079763789143851}{46179370926080}\hat{R}^{30}$$

$$-\frac{781322787957393546 07}{1899951260958720}\hat{R}^{32} - \frac{4717583293299314944 47}{3588796826255360}\hat{R}^{34} - \frac{592546736554605787}{525702660096}\hat{R}^{36}$$

$$-\frac{1278656698262280803109947}{385056788887633920}\hat{R}^{38} \quad . \quad . \quad . \tag{40}$$

As noted before, more terms can be easily generated as needed. Values for B_3', B_4' have been added to table 1. For values of B_4' that are small and within their uncertainties, we have listed them as $-0.000000(01)$ with uncertainty of the last two digit indicated in (..).

IV. TRUNCATED VIRIAL SERIES EQUATION OF STATE

We now have $[B_2(R_p), B_3(R_p), B_4(R_p)]$ and $[B_2'(R_p'), B_3'(R_p), B_4'(R_p)]$, to be used in truncated density virial series and pressure virial series, respectively. They can be employed to study the equation of state and probe the question of which truncated series is more accurate with the same number of coefficients? To provide benchmarks for this comparison, we have used extensive constant-pressure Monte Carlo simulations to provide new accurate data. The constant pressure Monte Carlo method used is standard and well documented[30]. We have taken great care to account for the finite number of particles used by using a range of number of particles and very long runs to ensure convergence. For each pressure, we used up to 3000 hardspheres and extrapolate the finite-size dependences to the large N limit. The number of configurations sampled can be as long as 10^{11} Monte Carlo steps per

particles. Typically 24 separate runs are used to estimate statistical errors. Our new results are consistent with previous published data of limited accuracy[9].

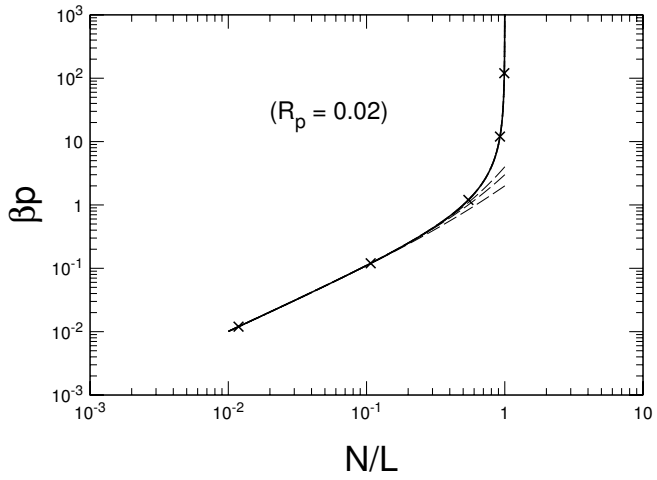

FIG. 2. Comparisons of linear pressure versus linear density plot for pore radius of $R_p = 0.52$ with Monte Carlo data. Monte Carlo data is denoted by X and the statistical errors are less than the size of the symbols. The truncated virial density series are denoted by three dashed lines. The lowest line has $n_{max} = 2$, then $n_{max} = 3$ and $n_{max} = 4$. n_{max} is the maximum order of virial coefficients used in the truncated series. The truncated virial pressure series are denoted similiarly by dotted, dashed and solid lines. The lines for the three different pressure series are very close to each other and not distinguishable in the plots. A more quantitative comparison is given in table II.

In figures 2,3 and 4, we compare pressure virial and density virial series expansions to Monte Carlo data, denoted by X. The statistical errors are less than the size of the symbols. Results for three different values of pore radii R_p are shown. They range from $R_p = 0.52$ very close to the one dimensional limit of 0.5, to $R_p = 0.90$ far from the one dimensional limit. For each pore radius, two sets of truncated series expansion predictions are plotted. The maximum order of the truncated series used is denoted by n_{max}. The density series are shown as three dashed lines. The lowest line has $n_{max} = 2$, then $n_{max} = 3$ and $n_{max} = 4$. The truncated pressure series are denoted similiarly by dotted, dashed and solid lines. It appears that the truncated pressure virial series describes the Monte Carlo data better than the truncated density virial series with the same number coefficients. See figures 2, 3 and 4. This should not be surprising, because the exact solution of the one dimensional hard rod fluid has $B'_n = 0$, for $n \geq 3$ versus $B_n = 1$ for all n. One would then expect, hardspheres in very narrow pores would be similiar. A truncated pressure series with all higher order set to zero would be better than similiar truncated density series. As the pressure increases,

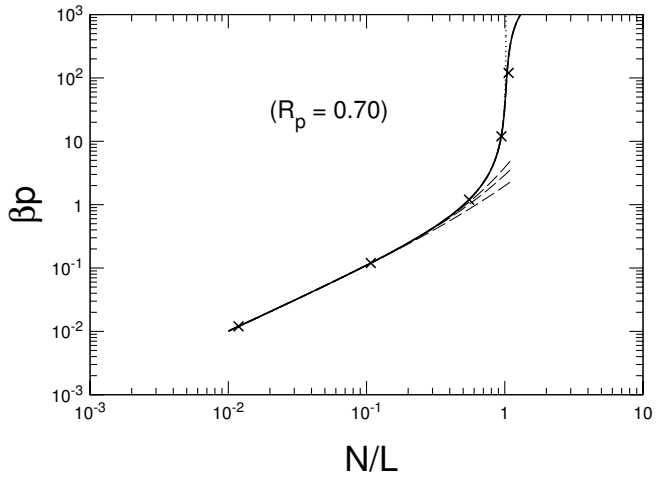

FIG. 3. Comparisons of linear pressure versus linear density plot for pore radius of $R_p = 0.70$ with Monte Carlo data. Monte Carlo data is denoted by X and the statistical errors are less than the size of the symbols. The truncated virial density series are denoted by three dashed lines. The lowest line has $n_{max} = 2$, then $n_{max} = 3$ and $n_{max} = 4$. n_{max} is the maximum order of virial coefficients used in the truncated series. The truncated virial pressure series are denoted similiarly by dotted, dashed and solid lines. The lines for the three different pressure series are very close to each other and not distinguishable in the plots. A more quantitative comparison is given in table II.

the truncated pressure series must also fail, consistent with the comparisons shown. Since the higher order B'_n increases with $\hat{R} = R_p - 1/2$, failure of the truncated pressure series is more serious with $R_p = 0.90$ at higher pressures. See figure 4. On the whole, the truncated pressure virial series provides a very good description of the crossovers from the one dimensional to narrow cylindrical pores at low and moderate pressures and densities. Observe that the truncation at $n_{max} = 3$ is already accurate over a wide range of pressure, density and pore sizes. This has the adventage that both B'_2, B'_3 are given analytically. For a more quantitative comparison, the nearest-neighbor longitudinal separation predictions and Monte Carlo data are presented in Table II.

V. REMARKS

In this paper, virial coefficients B_2 and B_3 were calculated analytically and numerical quadrature was used for B_4. They were also used to obtain the virial pressure series coefficients, B'_2, B'_3 and B'_4. This allows us to compare the truncated virial density and pressure series expansions to new accurate Monte Carlo data. Our comparisons shows that, the trun-

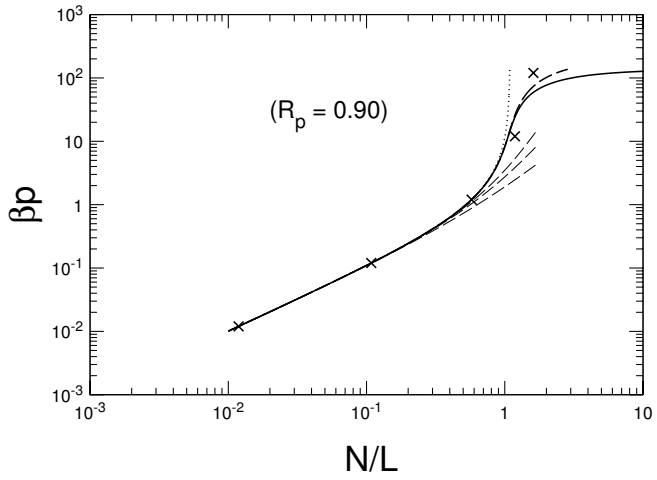

FIG. 4. Comparisons of linear pressure versus linear density plot for pore radius of $R_p = 0.90$ with Monte Carlo data. Monte Carlo data is denoted by X and the statistical errors are less than the size of the symbols. The truncated virial density series are denoted by three dashed lines. The lowest line has $n_{max} = 2$, then $n_{max} = 3$ and $n_{max} = 4$. n_{max} is the maximum order of virial coefficients used in the truncated series. The truncated virial pressure series are denoted similiarly by dotted, dashed and solid lines.

cated pressure virial series is accurate over a range of narrow pore widths, pressures and densities. The truncated pressure series is much better than the corresponding truncated density virial series. This dramatic difference is traced to the nature of the one dimensional hard sphere fluid's exact solution. These new results represent significant contributions to the long standing problem of fluids in narrow pores.

ACKNOWLEDGMENTS

This work used the Extreme Science and Engineering Discovery Environment (XSEDE), which is supported by National Science Foundation grant number OCI-1053575.

REFERENCES

1. J.A. Barker, Aust. J. Phys. **15**, 127(1962).

2. E.D.G Glandt, AIChE J. **27**, 51(1981).

3. P.E. Sokol, W.J. Ma, K.W. Herwig, W.M.Snow, Y. Wang, J. Koplik, and J.R. Banavar, Appl. Phys. Lett. **61**, 777(1992).

4. A.J. Post and D.A. Kofke, Phys. Rev. A, **45**, 939(1992)

TABLE II. Comparisons of linear pressure (βp) versus nearest-neighbor longitudinal separations $l(n_{max})$ of the truncated pressure virial series expansion predictions with Monte Carlo data. For three different pore radii of $0.52, 0.70$ and 0.90 , the maximum order virial coefficients used is denoted by n_{max}. The uncertainty of the MC data is in the last digit with magnitude indicated in (...)

R_p	βp	$l(2)$	$l(3)$	$l(4)$	$l(MC)$
0.52	120.000	1.00813085	1.00813085	1.00813330	1.0081293 (5)
0.52	12.000	1.08313306	1.08313306	1.08313330	1.083132 (3)
0.52	1.200	1.83313328	1.83313328	1.83313330	1.833135 (8)
0.52	0.120	9.33313330	9.33313330	9.33313330	9.33310 (2)
0.52	0.012	84.33313330	84.33313330	84.33313330	84.33 (1)
0.70	120.000	0.96261062	0.96261062	0.98798509	0.938224 (2)
0.70	12.000	1.06044765	1.06044765	1.06298509	1.05804 (1)
0.70	1.200	1.81273135	1.81273135	1.81298509	1.8126 (1)
0.70	0.120	9.31295972	9.31295972	9.31298509	9.31295 (3)
0.70	0.012	84.31298256	84.31298256	84.31298509	84.313 (1)
0.90	120.000	0.16322831	0.42242831	0.92179176	0.62097 (2)
0.90	12.000	0.94426342	0.94685542	0.99679176	0.84457 (2)
0.90	1.200	1.74177221	1.74179813	1.74679176	1.7376 (2)
0.90	0.120	9.24629214	9.24629240	9.24679176	9.2462 (2)
0.90	0.012	84.24674182	84.24674183	84.24679176	84.24 (1)

5. D.A. Kofke and A.J. Post, J. Chem. Phys. **98**, 4853(1993).

6. Q. Xin, I. Hiyne, and P. Siders, J. Chem. Soc., Faraday Trans. **90**, 973(1994).

7. K.E. Gubbins, M. Sliwinska-Bartkowiak, and S.H. Suh, Mol Simul. **17**, 333 (1996).

8. K.K. Mon and J.K. Percus, J. Chem. Phys. **112**, 3457 (2000)

9. I.E. Kamenetskiy, K.K. Mon and J.K. Percus, J. Chem. Phys. **121**, 7355(2004).

10. Ch. Forster, D. Mukamel, and H.A. Posch, Phys. Rev. E **69**, 066124(2004).

11. H. Kim, W.A. Goddard III, K.H. Han,C. Kim, E.K. Lee, P. Talkner, and P. Hänggi, J. Chem. Phys. **134**, 114502(2011).

12. K.K. Mon, J. Chem. Phys. **140**, 244504(2014).

13. M.J. Godfrey and M.A. Moore, Phys. Rev. E **89**, 032111(2014).

14. For a review and references see chapter 7 in, *Advanced Statistical Mechanics*, Barry M. McCoy (Oxford, Oxford, 2010). See also, *Statistical Mechanics*, R. Kubo (North Holland, Amsterdam, 1965).

15. For a review see, A.J. Masters, J. Phys.: Condens. Matter **20**, 283102(2008).

16. *Theory of Simple Liquids, 3rd Edition*, J.-P. Hansen and I.R. McDonald (Academic, New York, 2006).

17. *Statistical Mechanics*, J.E. Mayer and M.G. Mayer (Wiley, New York, 1940).

18. F.H. Ree and W.G. Hoover, J. Chem. Phys. **41**, 1635(1964). F.H. Ree and W.G. Hoover, J. Chem. Phys. **40**, 2048(1964).

19. R.J. Wheatley, Phys. Rev. Lett. **110**, 206601 (2013).

20. M. Bishop, Am. J. Phys. **51**, 1151(1983).

21. M. Luban and A. Baram, J. Chem. Phys. **76**, 3233(1982).

22. N.Clisby and B.M. McCoy, J. Stat. Phys., **122**, 15(2006).

23. M. Bishop, A. Masters, and J.H.R. Clarke, J. Chem. Phys. **110**, 11449(1999).

24 K.K. Mon and J.K. Percus, J. Chem. Phys. **110**, 2734(1999).

25. See, A. Bellemans, Physica **28**, 493 (1962). A. Bellemans, Physica **28**, 617 (1962). A. Bellemans, Physica **29**, 548 (1963). J. Stecki and S. Sokolowski, Mol. Phys. **39**, 343 (1980). S. Sokolowski and J. Stecki, Acta Phys. Pol. **A55**, 611 (1979). J. S. Rowlinson, Proceedings of the Royal Society of London. A. Mathematical and Physical Sciences **402**, 67 (1985). D.A. McQuarrie and J.S. Rowlinson, Mol. Phys. **60**, 977 (1987). For recent applications, see, J.H. Yang, A.J. Schultz, J.R. Errrington, and David A Kofke, J. Chem. Phys. **138**, 134706 (2013).

26. For a review and references see, P.S. Burada, P. Hänggi, F. Marchesoni, G. Schmid, and P.Talkner, ChemPhysChem. **10**, 45(2009). See also, L.D. Gelb, K.E. Gubbins, R. Radhakrishnan, and M. Sliwinska-Bartkowiak, Rep. Prog. Phys. **62**, 1573(1999).

27. *Numerical Recipes 3rd Edition: The Art of Scientific Computing* , W.H. Press, S.A. Teukolsky, W.T. Vetterling and B.P. Flannery (Cambridge, New York, 2007).

28. L. Tonks, Phys. Rev. **50**, 955(1936).

29. R.A. Dobbins, K. Mohammed, and D.A. Sullivan, J. Phys. Chem. Ref. Data, **17**, 1 (1988).

30. See, *Understanding Molecular Simulation*, D. Frenkel and B. Smit (Academic Press,New York, 2002).